JOC The Journal of Organic Chemistry

Article

pubs.acs.org/joc

Tuning the Electronic Properties of Nonplanar exTTF-Based Push–Pull Chromophores by Aryl Substitution

Raúl García,[†] Mª Ángeles Herranz,[†] Mª Rosario Torres,[‡] Pierre-Antoine Bouit,[§,∥] Juan Luis Delgado,[§] Joaquín Calbo,[⊥] Pedro M. Viruela,[⊥] Enrique Ortí,*[,⊥] and Nazario Martín*[,†,§]

[†]Departamento de Química Orgánica, Facultad de Química, Universidad Complutense de Madrid, 28040 Madrid, Spain

[‡]Centro de Asistencia a la Investigación de Rayos-X, Facultad de Ciencias Químicas, Universidad Complutense, Ciudad Universitaria, 28040 Madrid, Spain

[§]IMDEA-Nanociencia, Facultad de Ciencias, Universidad Autónoma, Cantoblanco, 28049 Madrid, Spain

[⊥]Instituto de Ciencia Molecular, Universidad de Valencia, 46980 Paterna, Spain

Supporting Information

ABSTRACT: A new family of π-extended tetrathiafulvalene (exTTF) donor–acceptor chromophores has been synthesized by [2 + 2] cycloaddition of TCNE with exTTF-substituted alkynes and subsequent cycloreversion. X-ray data and theoretical calculations, performed at the B3LYP/6-31G** level, show that the new chromophores exhibit highly distorted nonplanar molecular structures with largely twisted 1,1,4,4-tetracyanobuta-1,3-diene (TCBD) units. The electronic and optical properties, investigated by UV/vis spectroscopy and electrochemical measurements, are significantly modified when the TCBD acceptor unit is substituted with a donor phenyl group, which increases the twisting of the TCBD units and reduces the conjugation between the two dicyanovinyl subunits. The introduction of phenyl substituents hampers the oxidation and reduction processes and, at the same time, largely increases the optical band gap. An effective electronic communication between the donor and acceptor units, although limited by the distorted molecular geometry, is evidenced both in the ground and in the excited electronic states. The electronic absorption spectra are characterized by low- to medium-intense charge-transfer bands that extend to the near-infrared.

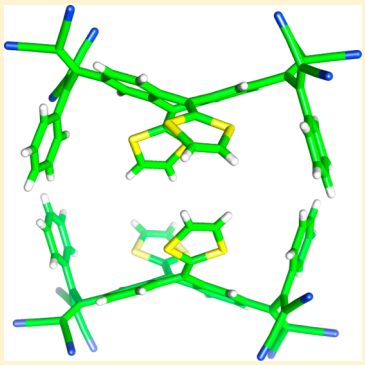

INTRODUCTION

The design and synthesis of novel charge-transfer (CT) chromophores with a control on the light-harvesting properties in the visible and near-infrared regions of the electronic spectra is currently a very active research area for a number of technological applications, particularly in fields such as nonlinear optics and photonics,[1] organic (plastic) photovoltaics,[2] dye-sensitized solar cells,[3] and more recently, small-molecule photovoltaic cells.[4] In this context, the electronic structure and geometrical features of a molecular electron-donor (D) unit can be strongly modified by the presence of a covalently connected electron-acceptor (A) group, which determines the appearance of new intramolecular charge-transfer (CT) bands in the electronic spectra of the D–A molecular entity.

A large variety of donor systems, involving molecular, oligomeric, and polymeric species such triarylamines, porphyrins, tetrathiafulvalene derivatives, oligophenylenvinylenes, and oligo- and polythiophenes, just to name a few, have been combined with different electron-acceptor moieties.[5] In order to get an efficient electronic communication between the donor and acceptor moieties, planarity has been recognized to be an important requirement. Therefore, most of the D-spacer-A molecules reported so far are geometrically planar or almost planar. In contrast, a scarce number of nonplanar donor–acceptor chromophores have been reported so far,[6] and only recently has the relationship existing between π-conjugation and the electronic properties in these push–pull molecules been systematically investigated.[7]

The singular electronic and geometrical features of π-extended tetrathiafulvalene (exTTF) have made this molecule one of the most useful and versatile electron donors, and therefore, exTTF derivatives have been widely used in the preparation of photo- and electroactive donor–acceptor dyads and triads,[8] molecular wires,[9] and materials for second- and third-order nonlinear optics,[10] as a building block in supramolecular chemistry,[11] and, more recently, for the realization of dye-sensitized solar cells.[12] In addition, exTTFs are pro-aromatic units,[13] with a characteristic butterfly shape distorted geometry[14] that, upon oxidation, experience a dramatic geometrical change resulting in a gain of aromaticity and planarity affording stable oxidized species.[15] Thus, the exTTF fragment looks particularly promising for modulating the conjugation between donor and acceptor units and controlling the electronic properties of new push–pull chromophores.

Received: September 18, 2012
Published: November 6, 2012

Diederich and co-workers have recently shown that alkynes substituted with suitable electron-donating groups readily undergo a [2 + 2] cycloaddition with powerful electron acceptors such as tetracyanoethylene (TCNE) and 7,7,8,8-tetracyano-*p*-quinodimethane (TCNQ),[16,17] followed by a retro-electrocyclization, to give nonplanar push−pull chromophores such as those depicted in Figure 1. This general

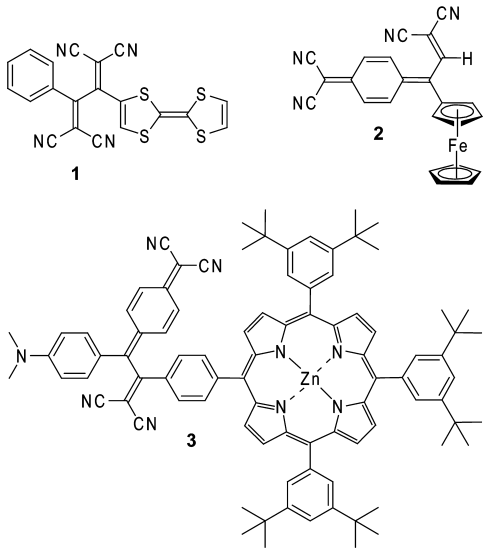

Figure 1. Representative examples of push−pull chromophores synthesized by cycloaddition−retro-electrocyclization processes between donor-activated alkynes and TCNE or TCNQ.

procedure, besides fulfilling all the requirements for a "click reaction" (atom economy, high yields, ambient conditions), provides easy access to functional materials, which, in principle, could feature enhanced physical properties such as better solubility, dispersibility, and sublimation capability when compared with their planar analogues. These enhanced properties are desirable for the easier preparation and processing of optoelectronic devices.[18]

In this work, we focus our attention on a new family of D-π-A chromophores in which exTTF and 1,1,4,4-tetracyanobuta-1,3-diene (TCBD) are covalently connected by using the electronically controlled [2 + 2] cycloaddition of TCNE with exTTF-substituted acetylenes, followed by retro-electrocyclization of the initially formed cyclobutenes (Schemes 1 and 2). Importantly, although the synthetic methodology is similar to that previously reported, the strong electron donor character and particularly the highly distorted geometry out of the planarity of curved exTTF should have a strong impact on the new push−pull chromophores. In this regard, the detailed electrochemical and optical characterization of compounds **7**, **8**, and **12** reveals the important effect that the acceptor moieties attached to the exTTF core have on the structure and optical properties of these chromophores. Density functional theory (DFT) calculations have been carried out to gain additional insight into the structural and electronic properties of these novel nonplanar push−pull chromophores. Theoretical predictions have been confirmed by experimental X-ray analysis of compound **12** bearing two acceptor units covalently connected to the central exTTF core.

Scheme 1. Synthesis of exTTF-TCBD Derivatives 7 and 8

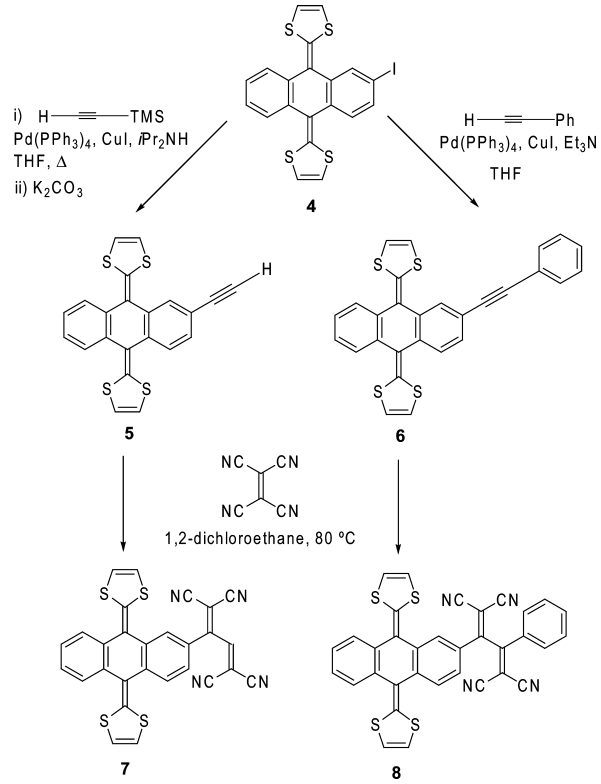

Scheme 2. Formation of the Doubly TCBD-Functionalized exTTF Derivative 12 by Sonogashira Coupling Followed by a [2 + 2] Cycloaddition−cycloreversion Reaction with TCNE

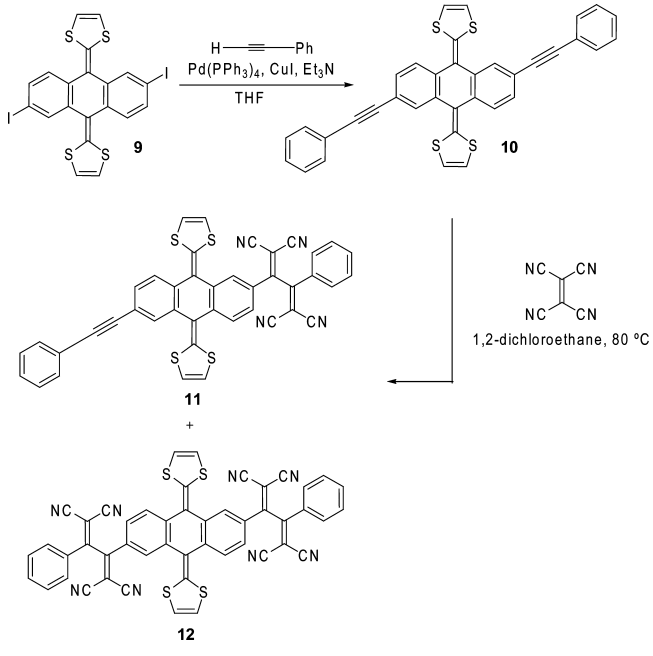

RESULTS AND DISCUSSION

Synthesis and Characterization. The synthesis of the push−pull chromophores **7** and **8** (Scheme 1) started with a Sonogashira coupling reaction of 2-iodo-9,10-bis(1,3-dithiol-2-ylidene)-9,10-dihydroanthracene (**4**)[19] with ethynyl(trimethyl)-silane to obtain compound **5**,[20] or with phenylacetylene, for the

dx.doi.org/10.1021/jo302047m | J. Org. Chem. 2012, 77, 10707−10717

Scheme 3. Proposed Mechanism for the Reaction of exTTF-Based Alkynes with TCNE

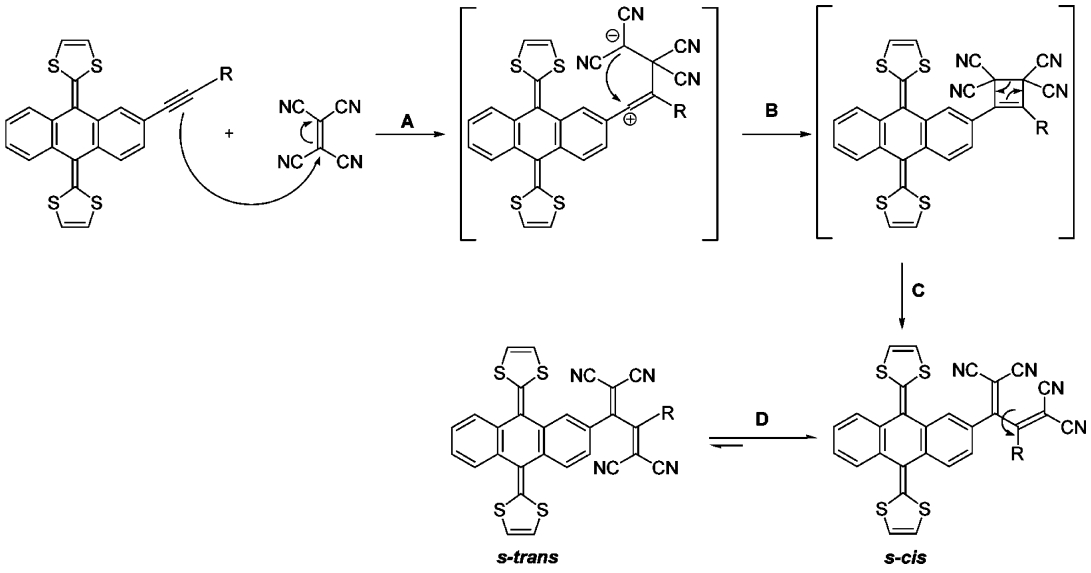

synthesis of **6**, in the presence of tetrakis(triphenylphosphine)-palladium(0) [$Pd(PPh_3)_4$], copper iodide, and diisopropylamine or triethylamine, followed by desilylation with K_2CO_3 for compound **5**. exTTFs **5** and **6** were obtained with a good overall yield (60−70%). The subsequent reaction of these exTTF-based alkynes with TCNE led to the target molecules after purification by column chromatography. Initial efforts to convert alkyne **6** to exTTF-TCBD **8** in refluxing benzene were unsuccessful. The reaction proceeds, however, when 1,2-dichloroethane was used as solvent. The fact that the starting alkyne **6** is sterically more hindered compared to **5** results in obtaining chomophore **7** in a higher yield (70%) than chromophore **8** (35%).

Scheme 2 outlines the synthesis of chromophore **12**, in which the initial Sonogashira coupling reaction of **9** with phenylacetylene in the presence of $Pd(PPh_3)_4$, CuI, and triethylamine afforded exTTF **10** in a good overall yield (65%). When derivative **10**, which bears two acetylenic moieties, was treated with a large excess (ca. 10 mmol) of TCNE, the expected bisadduct was formed, but the reaction did not proceed to completion. Monoadduct **11** was therefore obtained from the reaction, and the subsequent deactivation of the second alkyne unit makes the second addition very slow.[21] The doubly functionalized derivative **12** was only isolated in 35% yield after 5 days of reaction.

Based on the experimental outcome of the reactions and on the X-ray and theoretical structures discussed below, it is reasonable to assume that the mechanism for the reaction of exTTF-alkynes **5**, **6**, and **10** with TCNE consists of the four basic steps depicted in Scheme 3. From starting materials, the addition of one of the π-bonds of the alkyne to the electrophilic carbon situated between the two cyano groups produces a zwitterionic high-energy intermediate (step A). Subsequently, the ring-closed product is obtained through bond formation between the ionized carbons (step B). The thermally induced ring-opening cycloreversion step breaks the cyclobutene to give initially the *s-cis* product (step C) that eventually should isomerize to the *s-trans* conformer (step D).

The entire reaction profile for the transformation of dimethylanilinoacetylene with 1,1-dicyanoethene was computed by Diederich and co-workers in the gas phase and in solvated media.[22] A similar mechanism to the one proposed here was found to be occurring. In particular, substitution at the dicyanoethene lowered the energy of the ring-opening step by stabilizing the zwitterionic character of the transition state, with the net effect of making the first step rate-limiting when additional electro-accepting substituents are present in dicyanoethene.

In the case of exTTF-based alkynes, the first step seems to be the rate-limiting process by two additional reasons: (i) solvent effects: as previously discussed, reactions did not work at all in benzene, but when more polar solvents, that decrease the energy of this first transition state, were used (i.e., 1,2-dichloroethane), the reaction proceeds with good yields, and (ii) steric hindrance: the exTTF unit is a bulky substituent in the alkynes. In addition, when TCNE was replaced by TCNQ, the reaction does not occur with any of the exTTF-alkynes in solvents of different polarity, which could be accounted for by the added steric hindrance of TCNQ versus TCNE.

The synthesized exTTF-TCBD derivatives are colored and stable solids that can be stored for months in the laboratory without decomposition. They are also readily soluble in common organic solvents due to their sterically hindered structure that might reduce chromophore aggregation. The structural assignment of compounds is based on analytical and spectroscopic techniques (i.e., UV−vis, FTIR, ^{1}H NMR, ^{13}C NMR, and HRMS). In particular, compounds **7**, **8**, **11**, and **12** show the presence of strong cyano stretching vibrations at ~2200 cm^{-1} in the FTIR spectrum. ^{1}H and ^{13}C NMR spectra showed the expected signals for exTTF and TCBD moieties: the signals of the two 1,3-dithiole rings in the region of δ 6.6−6.3 of the ^{1}H NMR and the *sp* carbon atoms of the cyano groups at δ 114−110 in the ^{13}C NMR. For additional details, see the Experimental Section and Supporting Information.

Crystal and Molecular Structures. Crystals of **12** suitable for crystallographic analysis were grown by slow evaporation of a cooled hexane/CH_2Cl_2 1/1 solution. Molecules in the crystal structure of **12**, a mixed solvate with two molecules of CH_2Cl_2, arrange in a packing motif of pseudodimers with mutually recognizing bis(dithiole) anthraquinone moieties (Figure 2). Each dimer in the unit cell is constituted by two non-

dx.doi.org/10.1021/jo302047m | J. Org. Chem. 2012, 77, 10707−10717

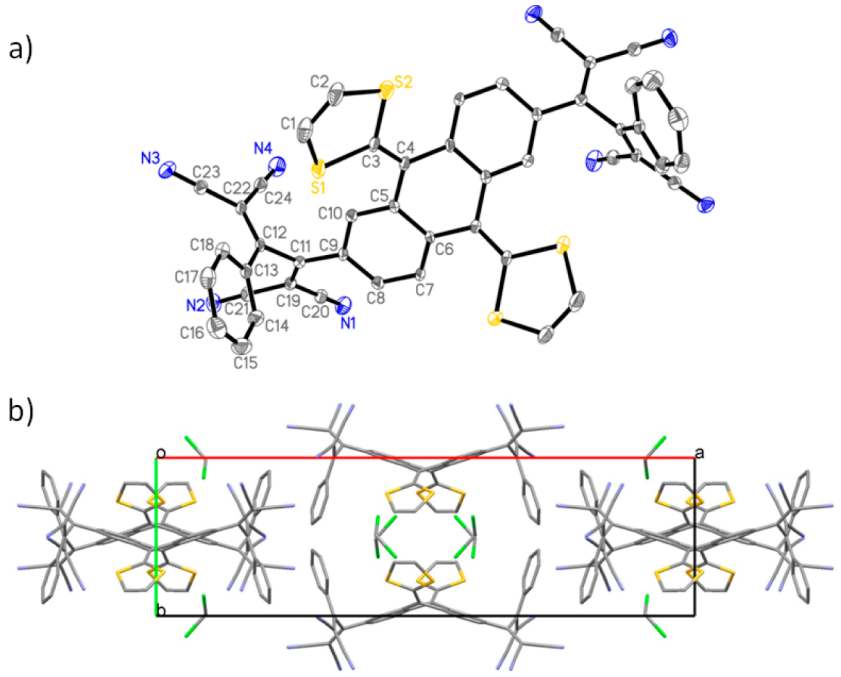

Figure 2. (a) ORTEP representation of the molecular structure of compound **12** with ellipsoids plotted at 20% probability level; H atoms omitted. (b) Crystal structure of **12**·CH_2Cl_2 showing the packing along the crystallographic "c" axis.

superimposable molecular enantiomers. Unfortunately, we were unable to produce single crystals of **7** and **8**.

Considerable nonplanarity is observed for the whole molecular structure of compound **12** and, especially, for the TCBD and exTTF moieties (see Figure 2 and Figure S5 and Table S1 in the Supporting Information for crystallographic parameters). The two dicyanovinyl units forming the TCBD moiety are almost orthogonal and define a dihedral angle (C19−C11−C12−C22) of −78.2 ± 0.7°, which compares with those previously reported for similar π-deconjugated D−A systems.[7,16] The *s-cis*-type conformation obtained for the TCBD units reflects the sterical role played by the exTTF moiety. This moiety makes the rotation around the single C11−C12 bond more difficult, and the *s-cis* conformer initially obtained from the ring-opening cycloreversion cannot evolve to the, in principle, more stable *s-trans* conformer (Scheme 3). The central ring of the anthracene unit is folded along the C4−C4′ axis into a boat conformation, and the exTTF moiety adopts a saddle-like structure in which the lateral benzene rings point upward and the dithiole rings point downward. This conformation is consistent with those observed from the crystal structures of different exTTF derivatives.[23]

The X-ray bond lengths measured for **12** (Table S2, Supporting Information) are of the expected order of magnitude for C−C bonds in conjugated or aromatic structures (1.40 ± 0.08 Å), for C−S bonds (1.737 ± 0.009 Å), and for C−N bonds (1.13 ± 0.02 Å). The shortest bond lengths correspond to the C1−C2 bonds of the dithiole rings (1.295 ± 0.011 Å) and to the exocyclic C3−C4 bonds linking the dithiole rings to the central anthracene unit (1.356 ± 0.008 Å).

The molecular structures of cromophores **7**, **8**, and **12** were theoretically optimized by using DFT calculations at the B3LYP/6-31G** level. An exhaustive conformational study was first performed for compounds **7** and **8** (see Figures S6 and S7 in the Supporting Information). In both cases, the most stable conformers correspond to twisted s-*trans* orientations of the TCBD unit. However, as shown in Scheme 3, the reaction mechanism provides the *s-cis* conformer after the thermal opening of the cyclobutene reaction intermediate, and due to the steric hindrance between the donor and acceptor units, the structure cannot evolve to the more stable *s-trans* conformation. This is in accord with the twisted *s-cis* dispositions that the TCBD units show in the crystal structure of compound **12** (Figure 2a). Figure 3, therefore, displays the minimum energy

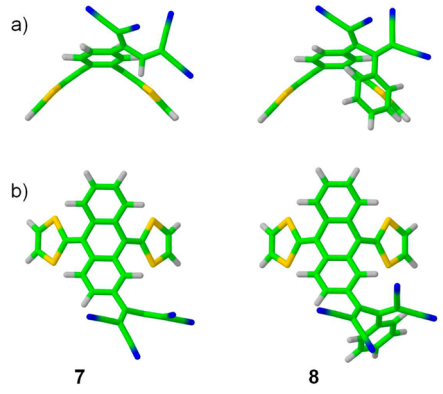

Figure 3. Mimimum energy *s-cis*-type conformations calculated for **7** and **8** at the B3LYP/6-31G** level. (a) Side view showing the saddle-like shape of the exTTF unit. (b) Top view.

conformations calculated for **7** and **8** with an *s-cis*-type orientation of the TCBD units (see Figure S8 for specific details about the optimized geometries). The conformation predicted for compound **12** has a C_2 symmetry axis passing through the center of the anthracene unit and is identical to the X-ray structure depicted in Figures 2a and S5 (Supporting Information).

As expected, the exTTF moiety has the typical saddle-like shape in all three compounds. The value calculated for the angle between the planes defined by the lateral benzene rings of

dx.doi.org/10.1021/jo302047m | J. Org. Chem. 2012, 77, 10707−10717

the anthracene unit has a similar value for the three compounds (**7**: 138.7°; **8**: 136.8°; **12**: 136.2°) and slightly underestimates the X-ray value obtained for **12** (142.6°) due to the packing interactions. The acceptor TCBD moieties are not coplanar with the benzene ring of the anthracene unit to which they are attached owing to the steric hindrance. The two dicyanovinyl halves of the TCBD units point upward in the opposite direction of the exTTF folding (Figure 3) and form a dihedral angle (C19−C11−C12−C22) of −54.2° for **7** that increases to −74.2° for **8** and −74.1° for **12** owing to the presence of the pendant phenyl substituents. The latter value is in good correlation with that observed from X-ray data (−78.2 ± 0.7°). The large twisting of the TCBD units breaks the conjugation between the two dicyanovinyl groups, and the C11−C12 bond lengthens to 1.473 Å for **7** and to 1.502 Å for **8** and **12** (X-ray value: 1.518 ± 0.008 Å). As discussed below, the limited π-conjugation of the TCBD unit largely influences the electronic and optical properties. The introduction of the phenyl substituent also has a significant effect on these properties.

Electrochemical Properties. Cyclic voltammetry (CV) and differential pulse voltammetry (DPV, see Figure S1, Supporting Information) experiments were carried out for **7**, **8**, and **12** and compared to exTTF and TCNE as reference compounds. Figure 4 displays the cyclic voltammograms recorded in THF for **7**, **8**, and **12**, and Table 1 summarizes the values of the redox potentials.

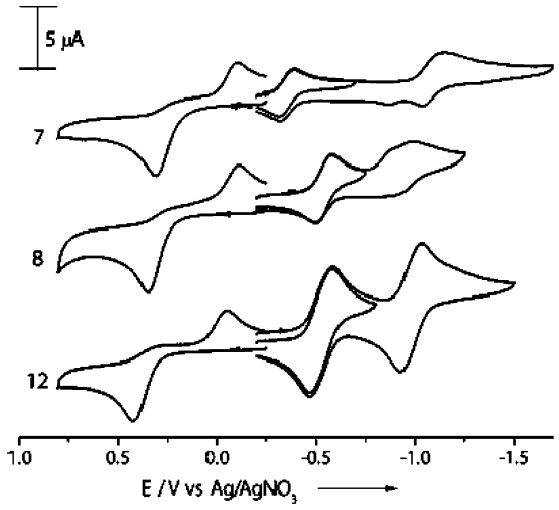

Figure 4. Cyclic voltammograms of compounds **7**, **8**, and **12** recorded in THF at a scan rate of 0.1 V s^{-1}, with 0.1 M $TBAPF_6$ as supporting electrolyte.

The exTTF-TCBD derivatives **7**, **8**, and **12** exhibit the characteristic two-electron quasi-reversible oxidation of exTTF[24] at gradually increasing positively shifted potentials (+307 mV for **7**, +346 mV for **8**, and +419 mV for **12**) and, in all cases, at higher potential values than the reference exTTF compound (+244 mV). Oxidation becomes more difficult due to the strong tetracyanobutadiene acceptor groups and, in the case of derivatives **8** and **12**, due to the more distorted geometry induced by the phenyl substitution.

The cyclic voltammograms of compounds **7** and **8** feature two well-resolved reversible reduction couples with similar currents for each peak ($1e^-$ each) centered on the tetracyanobutadiene acceptors. In the case of compound **12**, the peak current increases significantly due to the presence of two acceptor units (each reduction step implies $2e^-$). The cathodic shifts, compared to TCNE, observed in the first reduction potential originate from π-conjugation of the acceptor to the exTTF unit. The reduction processes are also strongly influenced by the introduction of phenyl substituents that increase the twisting of the TCBD unit and induce an additional loss of conjugation between the two acceptor halves of the TCBD unit. A smaller effect is also visible in the second reduction potentials. The difference between the first and second reduction potentials is larger for the exTTF-TCBD derivative **7** (746 mV), for which the two dicyanovinyl units are less twisted. In contrast, substitution of TCBD with phenyl groups, despite it induces a larger twisting between the two acceptor subunits, determines that the first and second reduction potentials become closer for both **8** (400 mV) and **12** (457 mV).

To control the performance of organic electronic devices, molecules with energetically low HOMO−LUMO energy gaps are of primary importance.[25] In this sense, compounds **7**, **8**, and **12** present small electrochemical gaps (~0.65−0.94 V), which can be easily tuned by the substituents incorporated in the TCBD unit.

Electronic Structure. Oxidized and Reduced Species. Figure 5 shows the atomic orbital (AO) composition of the highest occupied (HOMO−1 and HOMO) and lowest unoccupied (LUMO, LUMO+1, and LUMO+2) molecular orbitals of **8**. The HOMO and HOMO-1 are localized on the electron-donor exTTF unit, whereas the LUMO and LUMO+1 mainly spread over the acceptor TCBD moiety with some contribution from the anthracene skeleton. The pendant phenyl group also shows a small but important contribution to the LUMO and LUMO+1. The LUMO+2 is again localized on the exTTF moiety. The topology of the frontier MOs of chomophores **7** and **12** is equivalent to that described for **8**. For **7**, the contribution of the phenyl group does not exist and for **12** the LUMO and LUMO+1 are doubled due to the second TCBD group. The electronic communication between the donor and acceptor units is evidenced by the charge

Table 1. Cyclic Voltammetry Redox Potentials (THF, 0.1 M $TBAPF_6$) and Electrochemical and Optical Energy Gaps (E_g)

	$E^{pa}{}_{ox}{}^{b}$ (mV)	$E^{1/2}{}_{red,1}{}^{b}$ (mV)	$E^{1/2}{}_{red,2}{}^{b}$ (mV)	$\Delta E_{red}{}^{c}$ (mV)	$E_g(elect)^{d}$ (V)	onset^{e} (nm)	$E_g(opt)^{f}$ (eV)
exTTF[a]	+244						
TCNE		−240	−1112	1088			
7	+307	−348	−1094	746	0.65	1322	0.93
8	+346	−540	−940	400	0.87	929	1.33
12	+419	−524	−981	457	0.94	925	1.34

[a]exTTF = 2-[9-(1,3-dithiol-2-ylidene)anthracen-10(9*H*)-yilidene]-1,3-dithiole. [b]Potentials vs $Ag/AgNO_3$. Working electrode: glassy carbon; counter electrode: Pt; reference electrode: $Ag/AgNO_3$. Scan rate: 0.1 V s^{-1}. $E^{1/2} = (E^{pa} + E^{pc})/2$, where E^{pc} and E^{pa} are cathodic and anodic peak potentials, respectively. [c]$\Delta E_{red} = E^{1/2}{}_{red,1} - E^{1/2}{}_{red,2}$. [d]$E_g(elect) = E^{pa}{}_{ox} - E^{1/2}{}_{red,1}$. [e]Absorption onsets. [f]Optical energy gap.

dx.doi.org/10.1021/jo302047m | J. Org. Chem. 2012, 77, 10707−10717

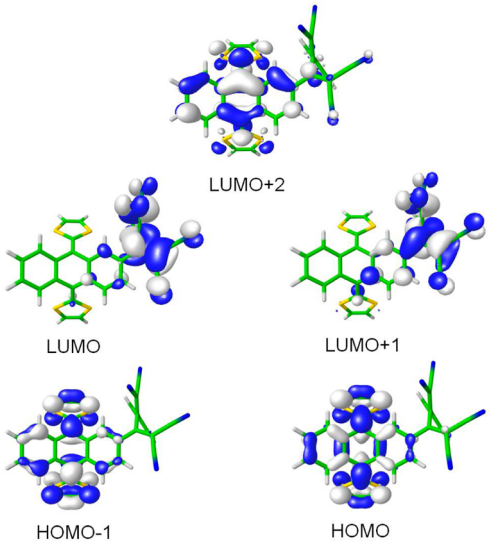

Figure 5. Electron density contours (0.03 e bohr^{-3}) calculated for the HOMOs and LUMOs of **8** at the B3LYP/6-31G** level.

transfer that takes place from the exTTF moiety to the TCBD unit. The latter supports a total charge of −0.21e for **7** that increases to −0.43e for **8** due to the additional charge transfer from the donor phenyl group. Attending to the nature of the HOMO and the LUMO, one can ensure that the lowest energy excitations in all three compounds will have a large charge-transfer character.

Figure 6 compares the molecular orbital energy distribution calculated for the exTTF molecule and for compounds **7**, **8**, and

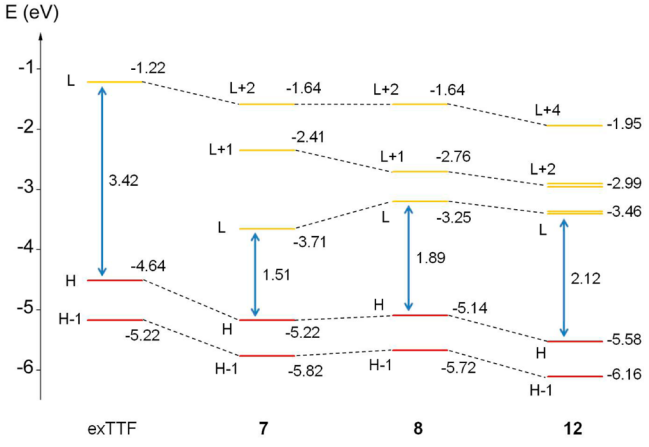

Figure 6. Energy diagram showing the energy values calculated for the highest occupied and lowest unoccupied molecular orbitals of exTTF, **7**, **8**, and **12**. H and L denote HOMO and LUMO, respectively.

12. The introduction of the acceptor TCBD group causes an energy lowering of the exTTF molecular orbitals that is more pronounced for **12** owing to attachment of the second TCBD group and provokes the appearance of low energy virtual orbitals (LUMO and LUMO+1 for **7** and **8**, LUMO to LUMO +3 for **12**) that are localized on the acceptor unit (see Figure 5). The stabilization of the HOMO justifies the higher oxidation potentials measured for compounds **7** (+0.307 V), **8** (+0.346 V), and **12** (+0.419 V) compared to exTTF (+0.244 V). However, the attachment of the donor phenyl group to the TCBD moiety produces an increase in the HOMO energy on passing from **7** (−5.22 eV) to **8** (−5.14 eV) that is not in good correspondence with the gradual increase of the oxidation potential along the series **7**, **8**, and **12**. The reason for this apparent discrepancy between experiment and theory is that Koopmans' theorem, which suggests that the higher the HOMO energy the easier the oxidation of the molecule, is a one-electron approach and does not apply to oxidation processes that involve two electrons as it is the case for exTTF derivatives.[8e,15c]

To further investigate the oxidized species, B3LYP/6-31G** calculations were performed for the dication species. The energy required to generate the dication augments along the series exTTF (9.81 eV), **7** (9.97 eV), **8** (10.07 eV), and **12** (10.32 eV), which is in agreement with the gradual increase recorded for the oxidation potential along this series. As depicted in Figure 7b, the minimum energy structure calculated

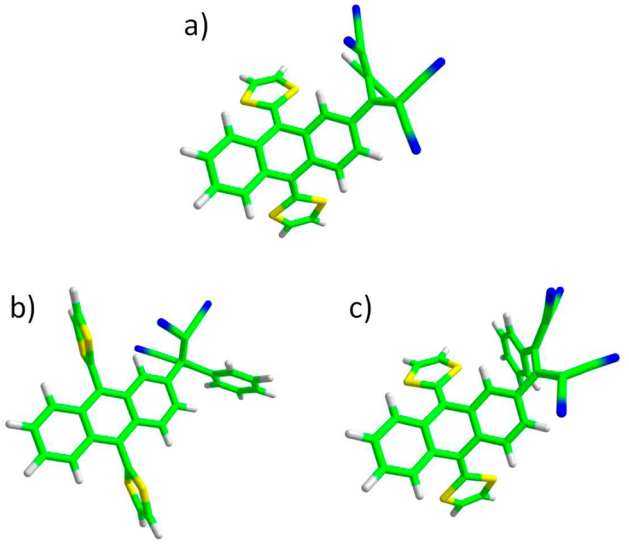

Figure 7. Minimum energy molecular structures calculated for (a) **8**, (b) $\mathbf{8}^{2+}$, and (c) $\mathbf{8}^{2-}$.

for $\mathbf{8}^{2+}$ corresponds to a conformation in which the TCBD is largely twisted (C19−C11−C12−C22: −89.8°) and the exTTF unit adopts an orthogonal conformation similar to those previously found for exTTF dications both theoretically and experimentally.[15,26] Upon oxidation, the exocyclic C3═C4 bonds that connect the dithiole rings to the anthracene unit elongate from 1.367 Å in neutral **8** to 1.485 Å in charged $\mathbf{8}^{2+}$ (averaged values) This lengthening allows for the rotation of the dithiole rings to minimize the steric interactions, and, as a consequence, the anthracene unit becomes planar and the dithiole rings lie perpendicular to the anthracene plane. For $\mathbf{8}^{2+}$, the exTTF moiety supports a total charge of +2.03e (+0.23e for neutral **8**) that is mainly concentrated on the dithiole rings (+1.43e). Similar structures are found for $\mathbf{7}^{2+}$ and $\mathbf{12}^{2+}$.

Concerning the reduced species, the energy calculated for the LUMO correctly reproduces the experimental trend observed for the first reduction potential. The LUMO energy increases in passing from **7** (−3.71 eV) to **8** (−3.25 eV) in agreement with the more negative potential measured for **8** (Table 1). This destabilization is ascribed to the attachment of the donor phenyl group to the TCDB unit that increases the twisting of the two $C(CN)_2$ subunits and thereby decreases the π-conjugation between them. In contrast, the LUMO+1 decreases in energy in passing from **7** (−2.41 eV) to **8** (−2.76 eV), and

dx.doi.org/10.1021/jo302047m | J. Org. Chem. 2012, 77, 10707−10717

the energy gap between the LUMO and LUMO+1 (LUMO+2 for **12**) significantly narrows (see Figure 6). Chromophore **7** presents a small HOMO−LUMO energy gap (1.51 eV) that widens for **8** (1.89 eV) and **12** (2.12 eV) in good agreement with the experimental trend measured for the electrochemical gap (Table 1).

The molecular geometries of the anion and dianion species were also optimized at the B3LYP/6-31G** level. Figure 7c displays the minimum energy structure calculated for $\mathbf{8}^{2-}$. The introduction of the extra electrons reduces the twisting of the TCBD unit (C19−C11−C12−C22 dihedral angle) from −74.2° in neutral **8** to −33.5° in $\mathbf{8}^{\bullet-}$ and −27.2° in $\mathbf{8}^{2-}$ due to the shortening of the central C11−C12 bond (**8**: 1.502 Å; $\mathbf{8}^{\bullet-}$: 1.433 Å; $\mathbf{8}^{2-}$: 1.421 Å). The extra electrons mainly enter the TCBD unit that accumulates a charge of −1.43e for $\mathbf{8}^{2-}$, but they are also placed in the adjacent phenyl rings due to their participation in the LUMO (see Figure 5). The pendant phenyl ring plays an important role in stabilizing the negative charge because it accommodates 0.33e in passing from **8** to $\mathbf{8}^{2-}$. This extra stabilization explains the positive shift of the second reduction potential in passing from **7** (−1.094 eV), for which the phenyl substituent is not present, to **8** (−0.940 eV) and **12** (−0.981 eV), and justifies the reduction of the difference between the first and second reduction potentials (Table 1).

Optical Properties. The UV/vis spectra of the exTTF-TCBD derivatives **7**, **8**, and **12** were recorded in diluted dichloromethane solutions and display the well-known absorptions of exTTF in the 400−440 nm visible region (Figure 8).[15,27] Additionally, new absorption features are

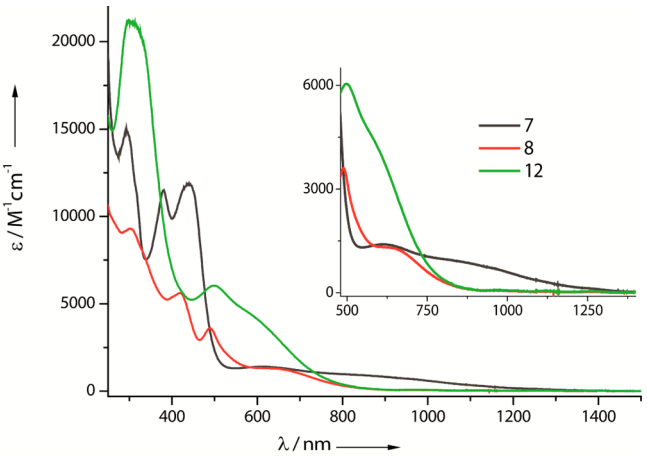

Figure 8. UV/vis spectra of exTTF-TCBD derivatives **7**, **8**, and **12** in CH_2Cl_2 (1×10^{-5} M).

observed in the red part of the spectrum (starting from 500 nm) with absorption onsets recorded in the NIR region (925−1325 nm). Low-energy optical gaps of 0.94−1.34 eV are therefore obtained in good linear correlation with the electrochemical gaps calculated from redox potentials (see Table 1). These low energy absorptions present low molar extinction coefficients (below 5000 M^{-1} cm^{-1}) and are assigned to CT transitions involving the donor exTTF and acceptor TCBD moieties. They exhibit a slight solvatochromism without any clear trend depending on solvent polarity (see Figures S2−S4, Supporting Information, for details).

To investigate the nature of the absorption bands observed in the electronic spectra, vertical transitions to the lowest energy singlet excited states (S_n) were calculated for **7**, **8**, and **12** using the time-dependent DFT (TD-DFT) approach and the B3LYP/6-31G**-optimized ground-state geometries. Table 2 summarizes the excited states with energies below 3.20 eV (wavelengths above 387 nm), which give rise to the absorption bands in the visible and near-infrared parts of the spectra. For compound **8**, TD-DFT calculations predict four states above 490 nm that result from electron excitations from the HOMO and HOMO−1, localized on the exTTF moiety, to the LUMO and LUMO+1, localized on the TCBD unit (see Figure 5). The four states imply an electron density transfer from the donor exTTF moiety to the acceptor TCBD unit and are, therefore, of CT nature. The S_2 and S_3 states are calculated close in energy at 1.96 eV (634 nm) and 2.06 eV (602 nm) with a total oscillator strength (f) of 0.086 and account for the broad absorption band centered at 656 nm. The S_4 state (2.53 eV, 490 nm) is more intense (f = 0.093) and correlates with the narrow band peaking at 491 nm. The S_1 state (HOMO→LUMO excitation) is calculated in the near-infrared (1.48 eV, 838 nm) and can be involved in the tail of the lowest energy band. The absorption band at 421 nm originates in the transition to the S_5 state (HOMO→LUMO+2) computed at 3.08 eV (403 nm) that is more intense (f = 0.212) and fully corresponds to the exTTF excitation (see Figure 5). Calculations therefore support that the first two bands centered around 650 and 490 nm correspond to CT bands.

Table 2. Lowest Energy Singlet Excited States Calculated for 7, 8, and 12 Using the TD-DFT Approach. Vertical Excitation Energies (E), Oscillator Strengths (f), Dominant Monoexcitations with Contributions (within Parentheses) Greater than 35%, and Description of the Excited State Are Summarized

	state	E (eV)[a]	f	monoexcitations[b]	description[c]
7	S_1	1.13 (1097)	0.046	H → L (98)	CT
	S_2	1.70 (729)	0.034	H−1 → L (98)	CT
	S_3	2.38 (521)	0.095	H → L+1 (95)	CT
	S_4	2.88 (430)	0.033	H−2 → L (86)	CT
	S_5	2.93 (423)	0.150	H−1 → L+1 (80)	CT
	S_6	3.11 (399)	0.028	H−3 → L (50)	CT
				H → L+2 (35)	exTTF
	S_7	3.14 (395)	0.117	H−3 → L (42)	CT
				H → L+2 (48)	exTTF
8	S_1	1.48 (838)	0.038	H → L (98)	CT
	S_2	1.96 (634)	0.042	H → L+1 (95)	CT
	S_3	2.06 (602)	0.044	H−1 → L (95)	CT
	S_4	2.53 (490)	0.093	H−1 → L+1 (98)	CT
	S_5	3.08 (403)	0.212	H → L+2 (92)	exTTF
12	S_1	1.71 (725)	0.017	H → L (98)	CT
	S_2	1.71 (725)	0.062	H → L+1 (98)	CT
	S_3	2.17 (571)	0.016	H → L+3 (98)	CT
	S_4	2.17 (571)	0.091	H → L+2 (95)	CT
	S_5	2.27 (545)	0.019	H−1 → L+1 (98)	CT
	S_6	2.27 (545)	0.069	H−1 → L (95)	CT
	S_7	2.69 (461)	0.033	H−1 → L+2 (96)	CT
	S_8	2.76 (450)	0.148	H−1 → L+3 (98)	CT
	S_9	3.19 (389)	0.149	H → L+4 (95)	exTTF

[a]Wavelengths (in nm) are given within parentheses. [b]H and L denote HOMO and LUMO, respectively. [c]CT indicates a charge-transfer exTTF → TCBD transition. exTTF denotes an exTTF-centered electronic transition.

dx.doi.org/10.1021/jo302047m | J. Org. Chem. 2012, 77, 10707−10717

The distribution of the excited states for compound **12** is identical to that discussed for **8**, but now there are eight CT states (S_1 to S_8) due to the presence of two TCBD units. The CT states appear by pairs and are calculated at higher energies than for **8** because of the higher energy gap between the HOMO/HOMO−1 and the LUMO to LUMO+3 orbitals (see Figure 6). The broad band observed in the visible region (450−800 nm) for **12** (Figure 8), which presents maximum absorption at 502 nm and a shoulder around 600 nm, is therefore assigned to CT electronic transitions. The excitation of the exTTF moiety is calculated at higher energies (state S_9, 3.19 eV, 389 nm) and is immersed under the low energy side of the broad and intense band centered around 300 nm (Figure 8).

For compound **7**, the absence of the donor phenyl group attached to the TCBD unit determines that the HOMO−LUMO energy gap has a value of 1.51 eV significantly smaller than for chromophores **8** and **12** (Figure 6). As a consequence, the HOMO→LUMO (state S_1) and HOMO−1→LUMO (S_2) excitations are calculated at very low energies (1.13 eV (1097 nm) and 1.70 eV (729 nm), respectively). This explains the long tail observed for the lowest-energy CT band of compound **7** that extends to 1325 nm. States S_3 to S_5 are also of CT nature and contribute to this band (S_3) and to the band peaking at 438 nm (S_4 and S_5). The excitation of the exTTF moiety is predicted around 390 nm mixed with other CT excitations (Table 2, states S_6 and S_7).

Calculations therefore predict that the absorption bands observed in the visible region for chromophores **7**, **8**, and **12** are mostly due to photoinduced charge-transfer transitions between the donor exTTF moiety and the acceptor TCBD unit. The intensity of these bands is relatively high because of the non-negligible overlap between the molecular orbitals of the exTTF moiety (HOMO and HOMO−1) and those of the TCBD unit (LUMO and LUMO+1) (Figure 5). Therefore, despite the highly distorted nonplanar structures exhibited by chromophores **7**, **8**, and **12**, an effective electronic communication takes place between the donor and acceptor units.

CONCLUSIONS

We have explored the strategy recently developed by Diederich and co-workers for the preparation of nonplanar push−pull-substituted buta-1,3-dienes, in combination with exTTF units. This methodology, which consists of a [2 + 2] cycloaddition of tetracyanoethene (TCNE) with electron-donor substituted alkynes and subsequent cycloreversion, has efficiently provided a new family of highly distorted exTTF-based push−pull chromophores. In addition, we have carried out an experimental and computational study on their electrochemical and optical absorption characteristics, which reveals the strong impact that aryl substitution plays in modulating the optoelectronic properties of the new chromophores.

Based on the X-ray crystal structure obtained for **12**, we were able to validate the mechanistic pathway of the reaction, which consists of a thermal conrotatory opening of the cyclobutene reaction intermediate that leads to the *s-cis* conformer. The largely twisted *s-cis*-type conformation adopted by the TCBD units in the crystal supports this mechanism and corroborates the prohibited interconversion of this conformer to the more stable *s-trans* owing to the steric hindrance between the donor and acceptor units.

Phenyl substitution of the acceptor TCBD units affects both the oxidation and reduction processes. Oxidation of exTTF is made more difficult both by the conjugation with the strong tetracyanobutadiene acceptor and by the additional sterical hindering induced by the phenyl ring. The reduction processes are strongly influenced by the introduction of phenyl substituents because they augment the twisting of the TCBD unit and provoke an additional loss of conjugation between the two acceptor dicyanovinyl halves of the TCBD unit.

Theoretical calculations carried out by using the DFT approach (B3LYP/6-31G**) forcefully support the experimental findings. The HOMO and HOMO−1 are localized on the exTTF moiety, and the introduction of the TCBD units determines the appearance of low-lying LUMO and LUMO+1 orbitals associated to these units. The electronic communication between the electron-donor and electron-acceptor fragments is supported both by the charge transfer that takes place between them for the neutral molecules and by their participation in the reduction and oxidation processes. The calculations performed for the dication, anion, and dianion species evidence the mutual influence of the donor and acceptor units and explain the experimental trends observed for the oxidation and reduction potentials.

The optical properties of compounds **7**, **8**, and **12** are characterized by low- to medium-intense absorption bands that completely cover the visible region and extend to the near-infrared. Theoretical calculations show that these bands are due to charge-transfer electronic transitions between the donor exTTF moiety and the acceptor TCBD units. The intensity of these CT bands is relatively high because, despite the highly distorted nonplanar structures exhibited by chromophores **7**, **8**, and **12**, an effective electronic communication takes place between the donor and acceptor units.

In summary, the new donor−acceptor chromophores **7**, **8**, and **12** exhibit interesting geometrical and electronic properties which can be tuned by the presence of an aryl group on the TCBD moiety. This strategy paves the way to the synthesis of more sophisticated push−pull exTTF derivatives where the substituent or functional group present on the starting alkyne determine the planarity, and hence the electronic properties, of the final chromophore.

EXPERIMENTAL SECTION

General Methods. All solvents were dried according to standard procedures. Reagents were used as purchased. 2-Iodo-9,10-bis(1,3-dithiol-2-ylidene)-9,10-dihydroanthracene (**4**),[19] 2-ethynyl-9,10-bis-(1,3-dithiol-2-ylidene)-9,10-dihydroanthracene (**5**),[20] and 2,6-diiodo-9,10-bis(1,3-dithiol-2-ylidene)-9,10-dihydroanthracene (**9**)[20] were prepared using described procedures. All air-sensitive reactions were carried out under argon atmosphere. Flash chromatography was performed using silica gel (230−240 mesh). Analytical thin-layer chromatography (TLC) was performed using aluminum-coated plates. NMR spectra were recorded on 300, 500, or 700 MHz spectrometers at 298 K using partially deuterated solvents as internal standards. Coupling constants (J) are denoted in Hz and chemical shifts (δ) in ppm. Multiplicities are denoted as follows: s = singlet, d = doublet, t = triplet, m = multiplet, br = broad. FT-IR spectra were recorded on a spectrometer suited with an ATR device. UV−vis spectra were recorded in CH_2Cl_2 solutions, with concentrations around 0.2 mM. The exact molecular weight of the new compounds was obtained by electrospray ionization mass spectra (ESI-MS) and matrix-assisted laser desorption ionization (coupled to a Time-Of-Flight analyzer) experiments (MALDI-TOF).

Electrochemistry. Electrochemical measurements were performed at room temperature in a potentiostate/galvanostate equipped with a home-built one-compartment cell with a three-electrode configuration, containing 0.1 M tetrabutylammonium hexafluorophosphate

($TBAPF_6$) as supporting electrolyte. A glassy carbon (GCE) was used as the working electrode, a platinum wire as the counter electrode, and a $Ag/AgNO_3$ nonaqueous electrode was used as reference. Prior to each voltammetric measurement the cell was degassed under an argon atmosphere by ca. 20 min. The solvent, THF, was freshly distilled from Na. The electrochemical measurements were performed using a concentration of approximately 0.2 mM of the corresponding compound.

2-(Phenylethynyl)-9,10-bis(1,3-dithiol-2-ylidene)-9,10-dihydroanthracene (6). To a solution of **4** (100 mg, 0.2 mmol) in dry THF (15 mL) under argon atmosphere were added $Pd(PPh_3)_4$ (12 mg, 0.01 mmol) and CuI (2 mg, 0.01 mmol) and subsequently phenylacetylene (0.02 mL, 0.2 mmol) and triethylamine (0.13 mL). The mixture was allowed to stir overnight and then was washed with NH_4Cl, H_2O, and brine. Afterward, the solvent was evaporated and the crude product purified by silica gel flash column chromatography (silica gel, hexane/dichloromethane 9:1 to 7:3) to afford product **6** as an orange solid (70% yield): Mp: 233−235 °C. ^1H NMR ($CDCl_3$, 300 MHz): δ = 7.86 (d, 1H, J = 1.7 Hz), 7.71 (m, 2H), 7.57 (m, 2H), 7.46 (m, 2H), 7.36 (m, 3H), 7.31 (m, 2H), 6.33 (s, 4H) ppm. ^{13}C NMR ($CDCl_3$, 75 MHz): δ = 135.6, 135.5, 134.5, 134.3, 134.2, 132.5, 130.6, 128.1, 127.3, 127.2, 126.9, 125.1, 125.1, 124.9, 124.0, 123.9, 122.4, 120.7, 120.5, 120.3, 119.6, 116.3, 116.2, 116.2, 88.7, 88.6 ppm. FTIR (KBr): ν = 2923, 2854, 1716, 1597, 1546, 1510, 1455, 1407, 1266, 1153, 1094, 1056, 833, 800, 755, 643 cm^{-1}. UV/vis (CH_2Cl_2): λ_{max} (log ε) = 376 (4.19), 424 (4.22), 440 (4.26) nm. HRMS (MALDI-TOF): calcd for $[C_{28}H_{16}S_4]^+$ 480.0129, found 480.0110.

2,6-Diphenylethynyl-9,10-bis(1,3-dithiol-2-ylidene)-9,10-dihydroanthracene (10). To a solution of **9** (250 mg, 0.4 mmol) in dry THF (25 mL) under argon atmosphere were added $Pd(PPh_3)_4$ (46 mg, 0.04 mmol) and copper iodide (8 mg, 0.04 mmol) and subsequently phenylacetylene (0.13 mL, 1.2 mmol) and triethylamine (0.3 mL). The mixture was allowed to stir overnight and then was washed with NH_4Cl, H_2O, and brine. Afterward, the solvent was evaporated and the crude product purified by silica gel flash column chromatography (silica gel, hexane/dichloromethane 9:1 to 7:3) to afford **10** as an orange solid (65% yield). Mp: 278−282 °C. ^1H NMR ($CDCl_3$, 300 MHz): δ = 7.87 (d, 2H, J = 1.50 Hz), 7.69 (d, 2H, J = 8.03 Hz), 7.56 (m, 4H), 7.46 (dd, 2H, J_1 = 8.03 Hz, J_2 = 1.50 Hz), 7.37 (m, 6H), 6.36, (s, 4H) ppm. ^{13}C NMR ($CDCl_3$, 75 MHz): δ = 136.6, 134.4, 134.2, 130.7, 128.2, 127.3, 127.2, 126.8, 123.9, 122.3, 119.7, 116.4, 88.6, 88.5 ppm. FTIR (KBr): ν = 2924, 2854, 1737, 1599, 1547, 1499, 1461, 1401, 1263, 1220, 769 cm^{-1}. UV/vis (CH_2Cl_2): λ_{max} (log ε) = 389 (4.17), 436 (4.25), 454 (4.31) nm. HRMS (MALDI-TOF): calcd for $[C_{36}H_{20}S_4]^+$ 580.0442, found 580.0428.

2-(Buta-1,3-diene-1,1,4,4-tetracyano)-9,10-bis(1,3-dithiol-2-ylidene)-9,10-dihydroanthracene (7). A mixture of **5** (100 mg, 0.24 mmol) and TCNE (31 mg, 0.26 mmol) dissolved in 1,2 dichloroethane (25 mL) was refluxed overnight under argon atmosphere. The solvent was evaporated, and the crude was purified by column chromatography on silica gel using dichloromethane as eluent to afford **7** as a dark green solid (95 mg, 70% yield). Mp > 300 °C. ^1H NMR ($CDCl_3$, 700 MHz): δ = 8.08 (s, 1H), 7.94 (d, 1H, J = 8.1 Hz), 7.76 (m, 2H), 7.66 (d, 1H, J = 1.8 Hz), 7.48 (dd, 1H, J_1 = 8.1 Hz, J_2 = 1.8 Hz), 7.36 (d, 1H, J = 5.7 Hz), 7.35 (d, 1H, J = 5.7 Hz), 6.41 (m, 4H) ppm. ^{13}C NMR (THF-d_8, 175 MHz): δ = 162.8, 155.6, 142.4, 141.6, 140.2, 138.1, 136.3, 136.3, 129.8, 128.4, 127.3, 127.3, 127.1, 126.8, 126.2, 126.1, 121.6, 121.1, 119.2, 119.1, 119.0, 118.4, 113.6, 113.3, 112.8, 110.6, 98.3, 91.0 ppm. FTIR (KBr): ν = 2961, 2923, 2853, 2225, 1594, 1543, 1501, 1451, 1335, 1093, 1022, 801, 756 cm^{-1}. UV/vis (CH_2Cl_2): λ_{max} (log ε) = 378 (4.21), 438 (4.24), 636 (3.25) nm. HRMS (MALDI-TOF): calcd for $[C_{28}H_{12}N_4S_4]^+$ 531.9939, found 531.9918.

2-(3-Phenylbuta-1,3-diene-1,1,4,4-tetracyano)-9,10-bis(1,3-dithiol-2-ylidene)-9,10 dihydroanthracene (8). To a solution of 50 mg (0.1 mmol) of **6** in 1,2-dichloroethane (20 mL) heated to 80 °C was added 73 mg (0.56 mmol) of TCNE under argon atmosphere. The mixture was allowed to stir for 3 days, and then the solvent was evaporated under reduced pressure and the crude was purified by column chromatography using dichloromethane as eluent, to afford product **8** as a dark blue solid (35% yield). Mp > 300 °C. ^1H NMR ($CDCl_3$, 300 MHz): δ = 8.02 (dd, 1H, J_1 = 8.5 Hz, J_2 = 2.3 Hz), 7.93 (d, 1H, J = 8.5 Hz), 7.76 (m, 3H), 7.70 (m, 2H), 7.59 (m, 3H), 7.35 (m, 2H), 6.47 (d, 2H, J = 2.1 Hz), 6.38 (d, 1H, J = 6.5 Hz), 6.33 (d, 1H, J = 6.5 Hz) ppm. ^{13}C NMR ($CDCl_3$, 75 MHz): δ = 168.1, 165.7, 143.5, 143.2, 142.4, 139.5, 137.4, 135.1, 135.0, 135.0, 131.6, 130.4, 130.0, 128.8, 128.0, 127.4, 127.1, 127.0, 126.6, 126.5, 125.5, 125.3, 120.9, 120.1, 118.6, 118.3, 118.2, 117.0, 112.6, 112.2, 112.1, 111.6, 88.0, 84.7 ppm. FTIR (KBr): ν = 2923, 2854, 2201, 1725, 1590, 1504, 1462, 1366, 1261, 1155, 805, 725, 554 cm^{-1}. UV/vis (CH_2Cl_2): λ_{max} (log ε) = 421 (3.75), 491 (3.56), 656 (3.12) nm. HRMS (MALDI-TOF): calcd for $[C_{34}H_{16}N_4S_4]^+$ 608.0252, found 608.0260.

Doubly TCBD Functionalization: General Method. 100 mg (0.17 mmol) of **10** were dissolved in 30 mL of 1,2-dichloroethane, and the solution was heated to 80 °C. A 240 mg (1.9 mmol) portion of TCNE was then added, and the reaction was allowed to stir for 5 days. Then, the solvent was removed under vacuum, and the crude products were separated and purified by column chromatography (silica gel, dichloromethane).

2-(3-Phenylbuta-1,3-diene-1,1,4,4-tetracyano)-6-(phenylethynyl)-9,10-bis(1,3-dithiol-2-ylidene)-9,10-dihydroanthracene (11). Dark blue solid (9 mg, 8% yield). Mp > 300 °C. ^1H NMR ($CDCl_3$, 300 MHz): δ = 8.02 (dd, 1H, J_1 = 8.7 Hz, J_2 = 2.1 Hz), 7.94 (d, 1H, J = 8.7 Hz), 7.91 (d, 1H, J = 1.3 Hz), 7.77 (dd, 2H, J_1 = 8.2 Hz, J_2 = 1.5 Hz), 7.71 (d, 1H, J = 7.5 Hz), 7.68 (d, 1H, J = 7.5 Hz). 7.59 (m, 4H), 7.50 (dd, 1H, J_1 = 8.0 Hz, J_2 = 1.5 Hz), 7.39 (m, 4H), 6.50 (s, 2H), 6.42 (d, 1H, J = 6.7 Hz), 6.36 (d, 1H, J = 6.7 Hz) ppm. ^{13}C NMR ($CDCl_3$, 75 MHz): δ = 168.0, 165.6, 144.2, 142.2, 140.5, 137.3, 135.2, 135.1, 134.9, 132.2, 132.1, 132.0, 131.6, 130.5, 130.1, 129.9, 128.9, 128.9, 128.8, 128.8, 128.1, 128.1, 127.5, 126.6, 126.5, 125.5, 123.5, 121.8, 120.0, 119.6, 118.7, 118.5, 118.3, 117.2, 112.6, 112.2, 112.1, 111.6, 90.6, 89.7, 88.0, 84.8 ppm. FTIR (KBr): ν = 2955, 2910, 2840, 2190, 1670, 1650, 1500, 1383, 1375, 1340, 1180, 990, 965, 606 cm^{-1}. UV/vis (CH_2Cl_2): λ_{max} (log ε) = 805 (2.28), 439 (3.23), 368 (3.77), 305 (3.68) nm. HRMS (MALDI-TOF): calcd for $[C_{42}H_{20}N_4S_4]^+$ 708.0565, found 708.0565.

2,6-Bis(3-phenylbuta-1,3-diene-1,1,4,4-tetracyano)-9,10-bis-(1,3-dithiol-2-ylidene)-9,10-dihydroanthracene (12). Dark blue solid (45 mg, 35% yield). Mp > 300 °C. ^1H NMR ($CDCl_3$, 500 MHz): δ = 7.95 (m, 4H), 7.84 (d, 2H, J = 1.9 Hz), 7.77 (m, 4H), 7.70 (m, 2H), 7.61 (m, 4H), 6.54 (d, 2H, J = 6.8 Hz), 6.48 (d, 2H, J = 6.8 Hz) ppm. ^{13}C NMR ($CDCl_3$, 125 MHz): δ = 167.9, 165.5, 146.2, 141.6, 136.8, 135.3, 131.5, 130.6, 129.9, 128.7, 127.9, 126.7, 126.3, 119.1, 118.4, 118.2, 112.4, 112.1, 111.9, 111.6, 88.0, 85.7 ppm. FTIR (KBr): ν = 2958, 2922, 2854, 2208, 1735, 1505, 1383, 1261, 1212, 1185, 1099, 1026, 805, 534 cm^{-1}. UV/vis (CH_2Cl_2): λ_{max} (log ε) = 502 (3.79), 606 (3.62) nm. HRMS (MALDI-TOF): calcd for $[C_{48}H_{20}N_8S_4]^+$ 836.0694, found 836.0652.

Computational Details. DFT calculations were carried out using the Gaussian 03 program package.[28]Geometry optimizations of both the neutral molecules and the dication, anion, and dianion species were performed with Becke's three-parameter B3LYP exchange-functional[29] and the 6-31G** basis set.[30] Anions of **7** and **8** were calculated as open-shell doublet systems using the unrestricted UB3LYP approach. Dications of **7**, **8**, and **12** and dianions of **7** and **8** were treated as closed-shell systems. Both neutral and charged species were also optimized in the presence of the solvent (THF, ε = 7.58) within the SCRF (self-consistent reaction field) theory using the polarized continuum model (PCM)[31] approach to model the interaction with the solvent. The PCM model considers the solvent as a continuous medium with a dielectric constant ε, and represents the solute by means of a cavity built with a number of interlaced spheres.[32] The solvent has a small influence on the optimized molecular geometries and all geometrical parameters quoted in the text correspond to values obtained in gas phase. The energies required to generate the dications were calculated as the difference between the total energies of the dication and the neutral molecule optimized in THF solution. Molecular orbitals were plotted using Chemcraft 1.6.[33]

Vertical electronic transition energies were computed at the B3LYP/6-31G** level using the TDDFT approach[34] and the

optimized ground-state molecular geometries. The vertical excitation energies were also calculated using the hybrid PBE0 functional,[35] which provides a similar description (energies and nature) of the lowest-energy excited states. For instance, the two first states of compound **7** were calculated at 1.28 eV (f = 0.050) and 1.88 eV (f = 0.039), respectively, slightly higher in energy than those predicted at the B3LYP level (see Table 2). However, both the B3LYP and the PBE0 functionals sometimes underestimate the energy of the CT excited states. This shortcoming of standard global hybrid functionals has been reported for donor−acceptor compounds for which there is a negligible overlap between the molecular orbitals involved in the excitation.[36] To solve the problem, the use of a long-range corrected functional as, e.g., the CAM-B3LYP functional,[37] is recommended. However, the CAM-B3LYP approach completely fails in reproducing the optical spectra of **7** since: (i) the lowest energy CT states are calculated too high in energy (for instance, S_1: 2.25 eV (551 nm); S_2: 2.92 (425 nm)), strongly underestimating the wavelength observed experimentally (600−800 nm) for the CT absorption band, and (ii) the CT states are computed to be among the most intense (f = 0.1−0.3) electronic transitions in contradiction with the low relative intensity of the CT band. The good performance of the B3LYP and PBE0 in describing the CT absorption bands of compounds **7**, **8**, and **12** is attributed to the non-negligible overlap between the molecular orbitals of the donor exTTF moiety and the acceptor TCBD unit (see Figure 5).

■ ASSOCIATED CONTENT

Supporting Information

^{1}H NMR, ^{13}C NMR, and HRMS (MALDI-TOF) spectra for all new compounds, DPVs, and absorption spectra in different solvents for **7**, **8**, and **12**, single-crystal structure of **12**, and theoretical calculations details. This material is available free of charge via the Internet at http://pubs.acs.org.

■ AUTHOR INFORMATION

Corresponding Author

*E-mail: enrique.orti@uv.es, nazmar@quim.ucm.es.

Present Address

[‖]Institut des Sciences Chimiques de Rennes, UMR 6226 CNRS, Université de Rennes 1, Campus de Beaulieu, 35042 Rennes Cedex, France.

Notes

The authors declare no competing financial interest.

■ ACKNOWLEDGMENTS

Financial support by MINECO of Spain (CTQ2011-24652, CT2009-08790, PIB2010JP-00196, 2010C-07-25200, and Consolider-Ingenio CSD2007-00010), FUNMOLS (FP7-212942-1), Generalitat Valenciana (PROMETEO/2012/053), and CAM (MADRISOLAR-2 S2009/PPQ-1533) is acknowledged. R.G. thanks the MECD for a FPU studentship. J.L.D. acknowledges the MINECO for a Ramón y Cajal fellowship cofinanced by the European Social Fund.

■ DEDICATION

Dedicated to the memory of our colleague Christian Claessens.

■ REFERENCES

(1) (a) Pron, A.; Gawrys, P.; Zagorska, M.; Djurado, D.; Demadrille, R. *Chem. Soc. Rev.* **2010**, *39*, 2577. (b) Koos, C.; Vorreau, P.; Vallaitis, T.; Dumon, P.; Bogaerts, W.; Baets, R.; Esembeson, B.; Biaggio, I.; Michinobu, T.; Diederich, F.; Freude, W.; Leuthold, J. *Nat. Photonics* **2009**, *3*, 216. (c) Sumalekshmy, S.; Henary, M. M.; Siegel, N.; Lawson, P. V.; Wu, Y.; Schmidt, K.; Brédas, J.-L.; Perry, J. W.; Fahrni, C. J. *J. Am. Chem. Soc.* **2007**, *129*, 11888.

(2) (a) Li, G.; Zhu, R.; Yang, Y. *Nat. Photonics* **2012**, *6*, 153−161. (b) Special issue on Organic Photovoltaics: *Acc. Chem. Res.* **2009**, *42*, 1689. (c) Fischer, M. K. R.; Wenger, S.; Wang, M.; Mishra, A.; Zakeeruddin, S. M.; Grätzel, M.; Bäuerle, P. *Chem. Mater.* **2010**, *22*, 1836. (d) Unger, E. L.; Ripaud, E.; Leriche, P.; Cravino, A.; Roncali, J.; Johansson, E. M. J.; Hagfeldt, A.; Boschloo, G. *J. Phys. Chem. C* **2010**, *114*, 11659. (e) Delgado, J. L.; Bouit, P.-A.; Filippone, S.; Herranz, M. A.; Martín, N. *Chem. Commun.* **2010**, *46*, 4853.

(3) (a) Ragoussi, M.-E.; Cid, J.-J.; Yum, J.-H.; de la Torre, G.; DiCenso, D.; Grätzel, M.; Nazeeruddin, M. K.; Torres, T. *Angew. Chem., Int. Ed.* **2012**, *51*, 4375−4378. (b) Bouit, P.-A.; Marszalek, M.; Humphry-Baker, R.; Viruela, R.; Ortí, E.; Zakeeruddin, S. M.; Grätzel, M.; Delgado, J. L.; Martín, N. *Chem.—Eur. J.* **2012**, *18*, 11621−11629. (c) Yella, A.; Lee, H.-W.; Tsao, H. N.; Yi, C.; Chandiran, A. K.; Nazeeruddin, M.; Diau, E. W.-H.; Yeh, Ch.-Y.; Zakeeruddin, S. M.; Grätzel, M. *Science* **2011**, *334*, 629−634.

(4) (a) Xiao, X.; Wei, G.; Wang, S.; Zimmerman, J. D.; Renshaw, C. K.; Thompson, M. E.; Forrest, S. R. *Adv. Mater.* **2012**, *24*, 1956−1960. (b) Lin, Y.; Li, Y.; Zhan, X. *Chem. Soc. Rev.* **2012**, *41*, 4245−4272. (c) Walker, B.; Kim, C.; Nguyen, T.-Q. *Chem. Mater.* **2011**, *23*, 470−482.

(5) (a) Walker, B.; Tamayo, A. B.; Dang, X.-D.; Zalar, P.; Seo, J. H.; Garcia, A.; Tantiwiwat, M.; Nguyen, T.-Q. *Adv. Funct. Mater.* **2009**, *19*, 3063. (b) Mayerhöffer, U.; Deing, K.; Gruß, K.; Braunschweig, H.; Meerholz, K.; Würthner, F. *Angew. Chem., Int. Ed.* **2009**, *48*, 8776. (c) Zhao, X.; Piliego, C.; Kim, B.; Poulsen, D. A.; Ma, B.; Unruh, D. A.; Fréchet, J. M. J. *Chem. Mater.* **2010**, *22*, 2325. (d) Fitzner, R.; Reinold, E.; Mishra, A.; Mena-Osteritz, E.; Ziehlke, H.; Körner, C.; Leo, K.; Riede, M.; Weil, M.; Tsaryova, O.; Weiß, A.; Uhrich, C.; Pfeiffer, M.; Bäuerle, P. *Adv. Funct. Mater.* **2011**, *21*, 897. (e) Jia, H. P.; Ding, J.; Ran, Y. F.; Liu, S. X.; Blum, C.; Petkova, I.; Hauser, A.; Decurtins, S. *Chem Asian J.* **2011**, *6*, 3312. (f) Zhang, J.; Wu, G.; He, C.; Deng, D.; Li, Y. *J. Mater. Chem.* **2011**, *21*, 3768. (g) El-Khouly, M. E.; Jaggi, M.; Schmid, B.; Blum, C.; Liu, S.-X.; Decurtins, S.; Ohkubo, K.; Fukuzumi, S. *J. Phys. Chem. C* **2011**, *115*, 8325.

(6) (a) Roncali, J.; Leriche, P.; Cravino, A. *Adv. Funct. Mater.* **2007**, *19*, 2045. (b) Pappenfus, T. M.; Schneiderman, D. K.; Casado, J.; López Navarrete, J. T.; Ruiz Delgado, M. C.; Zotti, G.; Vercelli, B.; Lovander, M. D.; Hinkle, L. M.; Bohnsack, J. N.; Mann, K. R. *Chem. Mater.* **2011**, *23*, 823.

(7) (a) Kato, S.-I.; Diederich, F. *Chem. Commun.* **2010**, *46*, 1994. (b) Yamada, M.; Rivera-Fuentes, P.; Schweizer, W. B.; Diederich, F. *Angew. Chem., Int. Ed.* **2010**, *49*, 3532. (c) Jordan, M.; Kivala, M.; Boudon, C.; Gisselbrecht, J.-P.; Schweizer, W. B.; Seiler, P.; Diederich, F. *Chem. Asian J.* **2011**, *6*, 396. (d) Breiten, B.; Wu, Y.-L.; Jarowski, P. D.; Gisselbrecht, J.-P.; Boudon, C.; Griesser, M.; Onitsch, C.; Gescheidt, G.; Schweizer, W. B.; Langer, N.; Lennartz, C.; Diederich, F. *Chem. Sci* **2011**, *2*, 88.

(8) (a) Bendikov, M.; Wudl, F.; Perepichka, D. F. *Chem. Rev.* **2004**, *104*, 4891. (b) Martín, N.; Sánchez, L.; Herranz, M. A.; Illescas, B.; Guldi, D. M. *Acc. Chem. Res.* **2007**, *40*, 1015. (c) Brunetti, F. G.; López, J. L.; Atienza, C.; Martín, N. *J. Mater. Chem.* **2012**, *22*, 4188. (d) Takano, Y.; Herranz, M. A.; Martín, N.; Gayathri Radhakrishnan, S.; Guldi, D. M.; Tsuchiya, T.; Nagase, S.; Akasaka, T. *J. Am. Chem. Soc.* **2010**, *132*, 8048. (e) Santos, J.; Illescas, B. M.; Martín, N.; Adrio, J.; Carretero, J. C.; Viruela, R.; Ortí, E.; Spänig, F.; Guldi, D. M. *Chem.—Eur. J.* **2011**, *17*, 2957.

(9) (a) Guldi, D. M.; Illescas, B. M.; Atienza, C. M.; Wielopolski, M.; Martín, N. *Chem.Soc. Rev.* **2009**, *38*, 1587. (b) Molina-Ontoria, A.; Wielopolski, M.; Gebhardt, J.; Gouloumis, A.; Clark, T.; Guldi, D. M.; Martín, N. *J. Am. Chem. Soc.* **2011**, *133*, 2370. (c) Wielopolski, M.; Santos, J.; Illescas, B. M.; Ortiz, A.; Insuasty, B.; Bauer, T.; Clark, T.; Guldi, D. M.; Martín, N. *Energy Environ. Sci.* **2011**, *4*, 765.

(10) Otero, M.; Herranz, M. A.; Seoane, C.; Martín, N.; Garín, J.; Orduna, J.; Alcalá, R.; Villacampa, B. *Tetrahedron* **2002**, *58*, 7463.

(11) (a) Pérez, E. M.; Martín, N. *Chem. Soc. Rev.* **2008**, *37*, 1512. (b) Huerta, E.; Isla, H.; Pérez, E. M.; Bo, C.; Martín, N.; de Mendoza, J. *J. Am. Chem. Soc.* **2010**, *132*, 5351. (c) Isla, H.; Gallego, M.; Pérez, E. M.; Viruela, R.; Ortí, E.; Martín, N. *J. Am. Chem. Soc.* **2010**, *132*, 1772.

(d) Grimm, B.; Santos, J.; Illescas, B. M.; Muñoz, A.; Guldi, D. M.; Martín., N. *J. Am. Chem. Soc.* **2010**, *132*, 17387. (e) Canevet, D.; Gallego, M.; Isla, H.; de Juan, A.; Pérez, E. M.; Martín, N. *J. Am. Chem. Soc.* **2011**, *133*, 3184.
(12) Wenger, S.; Bouit, P.-A.; Chen, Q.; Teuscher, J.; Di Censo, D.; Humphry-Baker, R.; Moser, J.-E.; Delgado, J. L.; Martín, N.; Zakeeruddin, S. M.; Grätzel, M. *J. Am. Chem. Soc.* **2010**, *132*, 5164.
(13) Andreu, R.; Galán, E.; Orduna, J.; Villacampa, B.; Alicante, R.; López Navarrete, J. T.; Casado, J.; Garín, J. *Chem.—Eur. J.* **2011**, *17*, 826.
(14) (a) Perepichka, D. F.; Bryce, M. R.; Perepichka, I. F.; Lyubchik, S. B.; Christensen, C. A.; Godbert, N.; Batsanov, A. S.; Levillain, E.; McInnes, E. J. L.; Zhao, J. P. *J. Am. Chem. Soc.* **2002**, *124*, 14227. (b) Christensen, C. A.; Batsanov, A. S.; Bryce, M. R. *J. Am. Chem. Soc.* **2006**, *128*, 10484.
(15) (a) Martín, N.; Sánchez, L.; Seoane, C.; Ortí, E.; Viruela, P. M.; Viruela, R. *J. Org. Chem.* **1998**, *63*, 1268. (b) Díaz, M. C.; Illescas, B. M.; Martín, N.; Viruela, R.; Viruela, P. M.; Ortí, E.; Brede, O.; Zilbermann, I.; Guldi, D. M. *Chem.—Eur. J.* **2004**, *10*, 2067. (c) Bouit, P.-A.; Villegas, C.; Delgado, J. L.; Viruela, P. M.; Pou-AméRigo, R.; Ortí, E.; Martín, N. *Org. Lett.* **2011**, *13*, 604.
(16) (a) Kato, S.-I.; Kivala, M.; Schweizer, W. B.; Boudon, C.; Gisselbrecht, J.-P.; Diederich, F. *Chem.—Eur. J.* **2009**, *15*, 8687. (b) Breiten, B.; Jordan, M.; Taura, D.; Zalibera, M.; Griesser, M.; Confortin, D.; Boudon, C.; Gisselbrecht, J.-P.; Schweizer, W. B.; Gescheidt, G.; Diederich, F. *J. Org. Chem.* **2012**, DOI: 10.1021/jo301194y.
(17) Fesser, P.; Iacovita, C.; Wäckerlin, C.; Vijayaraghavan, S.; Ballav, N.; Howes, K.; Gisselbrecht, J.-P.; Crobu, M.; Boudon, C.; Stöhr, M.; Jung, T. A.; Diederich, F. *Chem.—Eur. J.* **2011**, *17*, 5246.
(18) Walzer, K.; Maennig, B.; Pfeiffer, M.; Leo, K. *Chem. Rev.* **2007**, *107*, 1233.
(19) Díaz, M. C.; Illescas, B. M.; Seoane, C.; Martín, N. *J. Org. Chem.* **2004**, *69*, 4492.
(20) Illescas, B. M.; Santos, J.; Díaz, M. C.; Martín, N.; Atienza, C. M.; Guldi, D. M. *Eur. J. Org. Chem.* **2007**, 5027.
(21) For an exhaustive investigation about consecutive [2 + 2] cycloaddition−cycloreversion reactions in activated internal acetylenes, see: Silvestri, F.; Jordan, M.; Howes, K.; Kivala, M.; Rivera-Fuentes, P.; Boudon, C.; Gisselbrecht, J.-P.; Schweizer, W. B.; Seiler, P.; Chiu, M.; Diederich, F. *Chem.—Eur. J.* **2011**, *17*, 6088.
(22) Jarowski, P. D.; Wu, Y.-L.; Boudon, C.; Gisselbrecht, J.-P.; Gross, M.; Schweizer, W. D.; Diederich, F. *Org. Biomol. Chem.* **2009**, *7*, 1312.
(23) (a) Bryce, M. R.; Moore, A. J.; Hasan, M.; Ashwell, G. J.; Fraser, A. T.; Clegg, W.; Hursthouse, M. B.; Karaulov, A. I. *Angew. Chem., Int. Ed. Engl.* **1990**, *29*, 1450. (b) Jones, A. E.; Christensen, C. A.; Perepichka, D. F.; Batsanov, A. S.; Beeby, A.; Low, P. J.; Bryce, M. R.; Parker, A. W. *Chem.—Eur. J.* **2001**, *7*, 973. (c) Christensen, C. A.; Batsanov, A. S.; Bryce, M. R.; Howard, J. A. K. *J. Org. Chem.* **2001**, *66*, 3313.
(24) (a) Pérez, I.; Liu, S.-G.; Martín, N.; Echegoyen, L. *J. Org. Chem.* **2000**, *65*, 3796. (b) Herranz, M. A.; Yu, L.; Martín, N.; Echegoyen, L. *J. Org. Chem.* **2003**, *68*, 8379.
(25) Gautier, N.; Dumur, F.; Lloveras, V.; Vidal-Gancedo, J.; Veciana, J.; Rovira, C.; Hudhomme, P. *Angew. Chem., Int. Ed.* **2003**, *42*, 2765.
(26) Díaz, M. C.; Illescas, B. M.; Martín, N.; Perepichka, I. F.; Bryce, M. R.; Levillain, E.; Viruela, R.; Ortí, E. *Chem.—Eur. J.* **2006**, *12*, 2709.
(27) Guldi, D. M.; Sánchez, L.; Martín, N. *J. Phys. Chem. B* **2001**, *105*, 7139.
(28) Frisch, M. J.; Trucks, G. W.; Schlegel, H. B.; Scuseria, G. E.; Robb, M. A.; Cheeseman, J. R.; Scalmani, G.; Barone, V.; Mennucci, B.; Petersson, G. A.; Nakatsuji, H.; Caricato, M.; Li, X.; Hratchian, H. P.; Izmaylov, A. F.; Bloino, J.; Zheng, G.; Sonnenberg, J. L.; Hada, M.; Ehara, M.; Toyota, K.; Fukuda, R.; Hasegawa, J.; Ishida, M.; Nakajima, T.; Honda, Y.; Kitao, O.; Nakai, H.; Vreven, T.; Montgomery, J. A., Jr.; Peralta, J. E.; Ogliaro, F.; Bearpark, M.; Heyd, J. J.; Brothers, E.; Kudin, K. N.; Staroverov, V. N.; Kobayashi, R.; Normand, J.; Raghavachari, K.; Rendell, A.; Burant, J. C.; Iyengar, S. S.; Tomasi, J.; Cossi, M.; Rega, N.; Millam, J. M.; Klene, M.; Knox, J. E.; Cross, J. B.; Bakken, V.; Adamo, C.; Jaramillo, J.; Gomperts, R.; Stratmann, R. E.; Yazyev, O.; Austin, A. J.; Cammi, R.; Pomelli, C.; Ochterski, J. W.; Martin, R. L.; Morokuma, K.; Zakrzewski, V. G.; Voth, G. A.; Salvador, P.; Dannenberg, J. J.; Dapprich, S.; Daniels, A. D.; Farkas, O.; Foresman, J. B.; Ortiz, J. V.; Cioslowski, J.; Fox, D. J. *Gaussian 09*; Gaussian, Inc.: Wallingford, CT, 2009.
(29) (a) Lee, C.; Yang, W.; Parr, R. G. *Phys. Rev. B* **1988**, *37*, 785. (b) Becke, A. D. *J. Chem. Phys.* **1993**, *98*, 5648.
(30) Francl, M. M.; Pietro, W. J.; Hehre, W. J.; Binkley, J. S.; Gordon, M. S.; Defrees, D. J.; Pople, J. A. *J. Chem. Phys.* **1982**, *77*, 3654.
(31) (a) Tomasi, J.; Persico, M. *Chem. Rev.* **1994**, *94*, 2027. (b) Cramer, C. S.; Truhlar, D. G. *Solvent Effects and Chemical Reactivity*; Kluwer: Dordrecht, 1996; pp 1−80.
(32) (a) Miertus, S.; Scrocco, E.; Tomasi, J. *Chem. Phys.* **1981**, *55*, 117. (b) Miertus, S.; Tomasi, J. *J. Chem. Phys.* **1982**, *65*, 239. (c) Cossi, M.; Barone, V.; Cammi, R.; Tomasi, J. *Chem. Phys. Lett.* **1996**, *255*, 327. (d) Cances, E.; Mennucci, B.; Tomasi, J. *J. Chem. Phys.* **1997**, *107*, 3032. (e) Barone, V.; Cossi, M.; Tomasi, J. *J. Comput. Chem.* **1998**, *19*, 404. (f) Cossi, M.; Scalmani, G.; Rega, N.; Barone, V. *J. Chem. Phys.* **2002**, *117*, 43.
(33) http://www.chemcraftprog.com.
(34) (a) Casida, M. E.; Jamorski, C.; Casida, K. C.; Salahub, D. R. *J. Chem. Phys.* **1998**, *108*, 4439. (b) Jamorski, C.; Casida, M. E.; Salahub, D. R. *J. Chem. Phys.* **1996**, *104*, 5134. (c) Petersilka, M.; Grossmann, U. J.; Gross, E. K. U. *Phys. Rev. Lett.* **1996**, *76*, 1212.
(35) (a) Adamo, C.; Barone, V. *J. Chem. Phys.* **1999**, *110*, 6158. (b) Ernzerhof, M.; Scuseria, G. E. *J. Chem. Phys.* **1999**, *110*, 5029.
(36) (a) Wiggins, P.; Williams, J. A. G.; Tozer, D. J. *J. Chem. Phys.* **2009**, *131*, 091101. (b) Peach, P.; Benfield, M. J. G.; Helgaker, T.; Tozer, D. J. *J. Chem. Phys.* **2008**, *128*, 044118.
(37) Yanai, T.; Tew, D. P.; Handy, N. C. *Chem. Phys. Lett.* **2004**, *393*, 51.